CFD Simulation of Gas and Solids Mixing in FCC Strippers

Yingjie Liu, Xingying Lan, Chunming Xu, Gang Wang, and Jinsen Gao
State Key Laboratory of Heavy Oil Processing, China University of Petroleum, Beijing 102249, P.R. China

DOI 10.1002/aic.12646
Published online June 20, 2011 in Wiley Online Library (wileyonlinelibrary.com).

The gas and solid mixing in fluid catalytic cracking strippers with and without internals were investigated using computational fluid dynamics simulations. The Eulerian–Eulerian two-fluid model coupled with the modified Gidaspow drag model was used to simulate the gas-solid flow behavior. The grid independency study and the comparison of 2D and 3D simulations were carried out first. The residence time distribution model and axial dispersion model were utilized to obtain the parameters indicating the back-mixing degree, such as mean residence time, dimensionless variance and Peclet number of gas and solids. Moreover, the influence of bubble size and gas/solid flow distribution on the mass transfer between the bubble and emulsion phase were also analyzed. The results show that the baffles in the V-baffle stripper can efficiently enhance the gas and solids mixing, reduce the back-mixing degree of gas and solids, strengthen the mass transfer between the bubble and emulsion phase, and hence improve the stripping efficiency. © 2011 American Institute of Chemical Engineers *AIChE J,* 58: 1119–1132, 2012

Keywords: FCC stripper, gas-solid mixing, stripping efficiency, RTD, CFD

Introduction

Fluid catalytic cracking (FCC) is a key and widely used refinery process for converting heavy oils into valuable light products such as gasoline and diesel. Strippers are widely used in FCC units to remove or strip the hydrocarbons entrained and adsorbed on spent catalysts by the upward flowing steam. Insufficient stripping causes an additional combustion load imposed upon the regenerator with excessive heat production and a loss in final yield of valuable product. Thus the improvement of stripper operation draws extensive attention and numerous modifications have been undertaken to enhance stripper performance.

FCC strippers are generally operated in a gas-solid bubbling fluidized bed regime. For good strippers, it is desirable to realize effective gas and solid contact, to minimize short-circulating of solids and gas bypassing, to distribute the gas uniformly over the cross-section. Stripping efficiency is a strong function of gas-solid mixing characteristics such as bubble size, residence time distribution (RTD), backmixing degree, and gas/solid flow distribution. Therefore, an understanding of gas-solid mixing behavior in FCC strippers is essential for improving the stripping efficiency, which serves as a fundamental subject for the design and operation optimization of FCC strippers.

Many studies have been undertaken on gas-solid mixing phenomena in the gas-solid fluidization system. In bubbling fluidized beds, bubble characteristics is undoubtedly a very important influencing factor as the transport resistance is located on the surface of the bubbles. Nguyen et al.[1] found that the solid circulation occurred with down-flow at areas unoccupied by bubble tracks and up-flow in the wakes moving with the bubbles. These circulation cells were essentially formed by the action of the bubbles. Krishna and Baten[2] proposed that the axial dispersion coefficient of the dense phase was proportional to the centre-line solid velocity

Correspondence concerning this article should be addressed to J. Gao at jinsengao@yahoo.com.

which was influenced by the bubble rise velocity. The exchange coefficient between the bubble and solid phase was essential to solid mixing which decreases with the increase in bubble size.[3,4] The formation of large bubbles strongly decreased the exchange coefficient leading to mass transfer limitations. Krishna and Van Baten[5] suggested that the coalescence and break-up tendencies could significantly enhance the mass transfer rates. Overall, small bubbles should be preferred and the presence of large bubbles should be avoided to enhance the mass and energy exchange between gas and solid phases.[6,7]

To quantify the mixing degree in gas-solid bubbling bed, the tracer testing technology is widely used. The obtained RTD is of considerable importance in predicting the degree of back-mixing in gas-solid fluidized bed. Wolf and Resnick[8] investigated the RTD of solids in gas-solid countercurrent flow fluidized bed using magnetic sand as tracer. Sotudeh-Gharebaagh and Chaouki[9] studied the mixing and hydrodynamic behavior of a downward facing sparger in a turbulent fluidized bed by injecting the tracer into the bed. Du et al.[10] examined the gas and solid mixing characteristics in the bubbling and turbulent regimes of a gas-solid fluidized bed using helium and phosphor tracer techniques. Zhong et al.[11] studied the gas mixing in the spouted fluid bed injecting two different tracer gases. Experimental data obtained from tracer testing technologies are often fitted to appropriate models to characterize the mixing characteristics of the system. Smolders and Baeyens[12] used axial dispersed model and core/annulus model to describe the RTD curves in gas-solid circulating fluidized bed. Lorences et al.[13] characterized the divergence from the plug flow using the axial dispersion and n-CSTRs in series models via gas RTD experiments in the fixed and bubbling bed regime. Cui et al.[14] studied the axial gas and solid mixing at different positions of gas-solid fluid coker stripper with axial dispersion model using helium and treated catalyst as tracers.

Recently, computational fluid dynamics (CFD) has become a valuable tool for studying the flow in complex multiphase systems, including gas-liquid systems,[15–17] gas-solid dilute phase beds like circulating fluidized bed[18,19] and gas-solid dense beds with relative big particles like Geldart B.[20] Despite remarkable progress in CFD modeling of gas-solid fluidized beds, just a little numerical work on gas and solids mixing in fluidized beds has been reported in the literature, and few numerical studies address the gas and solids mixing in bubbling beds with Geldart A particles.

With heavier feedstocks processed in the FCC units, more hydrocarbons are brought into the strippers. The conventional FCC strippers without internals no longer meet the stripping requirement because of severe back-mixing. Internals such as V-baffle and disk-donut baffle were then assembled in to the column to increase the gas-solid contact and improve the stripping efficiency. O'Dowd[21] found that the solid mixing degree in a baffled column was greater than that in an unbaffled column at comparable operating conditions in the slurry bubble column. Cui et al.[22] reported that horizontal or inclined baffles increased the gas-solid contact and reduced the axial dispersion, thereby increased the stripping efficiency. Xia et al.[15] also found that the inclusion of horizontal baffles or corrugated packing could dampen the effect of global back-mixing. Zhang et al.[23] suggested that compared to the baffle-free column, the axial solid dispersion coefficient was significantly reduced when multilayer louver baffles were inserted in the gas-solid fluidized bed. Therefore, the development and improvement of new internals with high efficiency primarily depends on the quantitative understanding of gas-solid mixing characteristics such as bubble size, RTD, backmixing degree, and gas/solid flow distribution.

Our research group had successfully undertaken experimental and computational studies of mass transfer characteristics and stripping efficiency of bubbling fluidized beds in FCCU strippers.[24,25] Based on the previous research, this article focuses on the investigation of gas and solids mixing characteristics in FCC strippers, and the quantitative analyses of influence of gas and solids mixing on stripping efficiency. Bubble feature, characteristics of transient local voidage and velocities, and RTDs of gas and solid are examined. The parameters characterizing overall back-mixing degree and local back-mixing index were obtained and compared with the available experimental data.

Mathematical Models

Governing equations and constitutive relations

The Eulerian–Eulerian method is widely applied to the modeling of the dense phase bubbling bed. This model treats both the gas and solid phase mathematically as continuous and fully interpenetrating. Generalized Navier-Stokes equations are used for the interacting continua. To close the governing equations, the constitutive relations are needed. Because the solid phase is treated as continuous, it has similar properties to a continuous fluid. By using the kinetic theory of granular flows,[26–28] the viscous forces and the solid pressure of the particulate phase can be described as a function of the so-called granular temperature. The Eulerian–Eulerian method using the kinetic theory for granular flow has shown its suitability for modeling dense gas-solid fluidized beds.[29,30] The governing equations and constitutive relations are shown in Table 1.

Gas-solid drag model

The gas-solid drag model which represents the interaction of the gas and particulate phase is key to a successful simulation. For the bubbling bed with Geldart A particles, the widely used Gidaspow drag model[28] employing the Ergun equation[31] for dense phase calculation and the Wen-Yu equation[32] for dilute phase calculation always overestimated the bed expansion. Gao et al.[24,25] proposed a modified Gidaspow drag model based on the equivalent diameter obtained by Lettieri et al.[33] and successfully simulated the hydrodynamic characteristics in bubbling fluidized beds (FCCU strippers). The gas-solid drag model proposed by Gao et al.[24,25] was therefore applied in this article and shown in Table 1.

RTD model

Numerical tracing methods similar to the experimental tracing methods were used to obtain the RTDs of gas and solid phase. The gas/solid tracer which had the same

Table 1. Governing Equations and Constitutive Correlations

Conservation equations

Gas-phase continuity equation $\frac{\partial}{\partial t}(\alpha_g \rho_g) + \frac{\partial}{\partial x_j}(\alpha_g \rho_g u_{gj}) = 0$

Solid-phase continuity equation $\frac{\partial}{\partial t}(\alpha_p \rho_p) + \frac{\partial}{\partial x_j}(\alpha_p \rho_p u_{pj}) = 0$

Gas-phase momentum equation $\frac{\partial}{\partial t}(\alpha_g \rho_g u_{gj}) + \frac{\partial}{\partial x_j}(\alpha_g \rho_g u_{gi} u_{gj}) = -\alpha_g \frac{\partial p}{\partial x_j} + \frac{\partial \tau_{g,ij}}{\partial x_j} + \alpha_g \rho_g g_i - \beta(u_{gi} - u_{pi})$

Solid -phase momentum equation $\frac{\partial}{\partial t}(\alpha_p \rho_p u_{pj}) + \frac{\partial}{\partial x_j}(\alpha_p \rho_p u_{pi} u_{pj}) = -\alpha_p \frac{\partial p}{\partial x_j} + \frac{\partial \tau_{p,ij}}{\partial x_j} + \alpha_p \rho_p g_i - \beta(u_{pi} - u_{gi})$

Species transport equation in gas phase $\frac{\partial}{\partial t}(\alpha_g \rho_g Y_{g,n}) + \frac{\partial}{\partial x_j}(\alpha_g \rho_g u_{gj} Y_{g,n}) = \frac{\partial}{\partial x_j}\left(\alpha_g \rho_g D \frac{\partial}{\partial x_j} Y_{g,n}\right)$

Species transport equation in solid phase $\frac{\partial}{\partial t}(\alpha_p \rho_p Y_{p,n}) + \frac{\partial}{\partial x_j}(\alpha_p \rho_p u_{pj} Y_{p,n}) = \frac{\partial}{\partial x_j}\left(\alpha_p \rho_p D \frac{\partial}{\partial x_j} Y_{p,n}\right)$

Solid-phase turbulent fluctuating energy equation $\frac{3}{2}\left[\frac{\partial}{\partial t}(\rho_p \alpha_p \Theta) + \frac{\partial}{\partial x_k}(\rho_p \alpha_p \vec{v}_p \Theta)\right] = \mu_p\left(\frac{\partial u_{pk}}{\partial x_i} + \frac{\partial u_{pi}}{\partial x_k}\right)\frac{\partial u_{pk}}{\partial x_i} + \frac{\partial}{\partial x_k}(\Gamma_\Theta \frac{\partial \Theta}{\partial x_k}) - p_p \frac{\partial u_{pk}}{\partial x_k} - \gamma_\Theta$

Constitutive correlations

Gas-phase stress tensor $\tau_{g,ij} = \mu_g\left(\frac{\partial u_{gj}}{\partial x_i} + \frac{\partial u_{gi}}{\partial x_j}\right)$

Solid-phase stress tensor $\tau_{p,ij} = \mu_p\left(\frac{\partial u_{pj}}{\partial x_i} + \frac{\partial u_{pi}}{\partial x_j}\right) + \left(\lambda_p - \frac{2}{3}\mu_p\right)\frac{\partial u_{pk}}{\partial x_k}\delta_{ij} - p_p \delta_{ij}$

Solid-phase pressure $P_p = \alpha_p \rho_p \Theta + 2\rho_p(1+e)\,\alpha_p^2 g_0 \Theta$

Granular temperature $\Theta = \frac{1}{3}\left\langle \overline{u_p' u_p'} \right\rangle$

Radial distribution function $g_0 = \left[1 - \left(\frac{\alpha_p}{\alpha_{p,max}}\right)^{\frac{1}{3}}\right]^{-1}$

Solid-phase shear viscosity $\mu_p = \frac{10\,\rho_p\, d_p \sqrt{\pi\,\Theta}}{96\,(1+e)\,g_0}\left[1 + \frac{4}{5}\,(1+e)\,g_0 \alpha_p\right]^2 + \frac{4}{5}\alpha_p^2 \rho_p d_p g_0 (1+e)\sqrt{\frac{\Theta}{\pi}}$

Solid-phase bulk viscosity $\lambda_p = \frac{4}{3}\alpha_p \rho_p d_p g_0 (1+e)\sqrt{\frac{\Theta}{\pi}}$

Diffusion coefficient $\Gamma_\Theta = \frac{150\,\rho_p d_p \sqrt{\pi\Theta}}{384\,(1+e)\,g_0}\left[1 + \frac{6}{5}\,(1+e)\,g_0\,\alpha_p\right]^2 + 2\alpha_p^2 \rho_p d_p g_0\,(1+e)\sqrt{\frac{\Theta}{\pi}}$

Collisional dissipation energy fluctuation $\gamma = 3\,(1-e^2)\alpha_p^2 \rho_p g_0 \Theta\left[\frac{4}{d_p}\sqrt{\frac{\Theta}{\pi}} - \frac{\partial u_{pk}}{\partial x_k}\right]$

Drag model For $\alpha_g > 0.8$, $\beta = \frac{3}{4}C_D \frac{a_p a_g \rho_g \left|\vec{u}_p - \vec{u}_g\right|}{d_p^*} a_g^{-2.65}$

For $\alpha_g \le 0.8$, $\beta = 150\frac{a_p(1-a_g)\mu_g}{a_g\left(d_p^*\right)^2} + 1.75\frac{\rho_g a_p \left|\vec{u}_p - \vec{u}_g\right|}{d_p^*}$

where $C_D = \begin{cases} \frac{24}{Re_p}\,(1 + 0.15\,Re_p^{0.687}) & (Re_p \le 1000) \\ 0.44 & (Re_p > 1000) \end{cases}$ $Re_p = \frac{a_g \rho_g d_p^* |\vec{u}_g - \vec{u}_p|}{\mu_g}$

properties with the stripping gas/catalyst was injected into the gas/catalyst inlet after the steady flow behavior was obtained, and the tracer concentration was monitored at the gas/catalyst outlet to obtain the corresponding RTD.

The RTD function $E(t)$ is calculated as

$$E(t) = Y_n(t) \Big/ \int_0^\infty Y_n(t)dt \tag{1}$$

The mean residence time t_m is calculated by integrating the RTD as

$$t_m = \int_0^\infty tE(t)dt \tag{2}$$

The variance of the standard deviation σ_t^2 of the RTD is

$$\sigma_t^2 = \int_0^\infty (t - t_m)^2 E(t)dt \tag{3}$$

The dimensionless variance σ_θ^2 is calculated using

$$\sigma_\theta^2 = \sigma_t^2 / t_m^2 \tag{4}$$

Axial dispersion model

The axial dispersion model proposed by Danckwerts[34] was widely used in the evaluation of the RTD characteristics.[35–38] Despite the evidence that a convective mechanism may be dominating in fluidized bed with core-annular phenomena,[39] the dispersion model can still get acceptable agreements with experimental results.[12] Grasa and

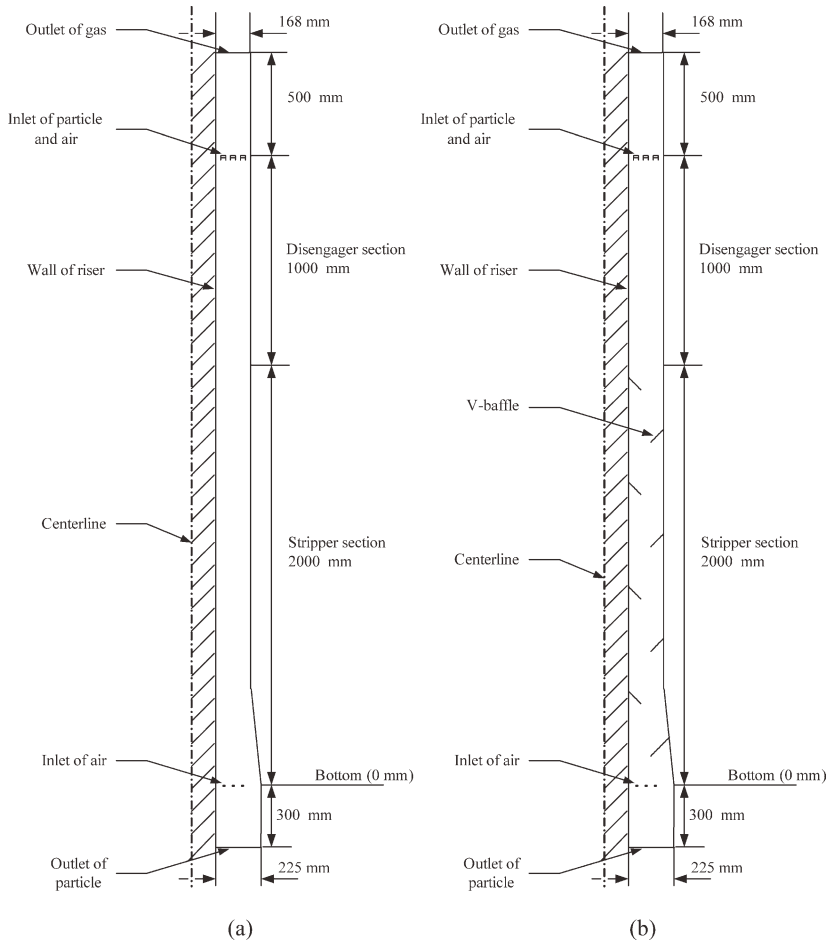

Figure 1. (a) Structure of the cylinder stripper. (b) Structure of the V-baffled stripper.

Abanades[40] compared the dispersion model and the countercurrent back-mixing model to describe the axial solid mixing in fluidized beds and found that the axial dispersion model was capable to fit the majority of experiments well.

The axial dispersed model assumes the fluid to be in plug flow with axial dispersion superimposed on it. The model lumps the different mechanisms of mixing into a single axial dispersion coefficient D_{ax}, or its dimensionless Peclet number Pe. Pe ranges from 0 to $+\infty$. Bigger Pe represents to a smaller degree of back-mixing.

The relation between Pe and D_{ax} is

$$Pe = \frac{uL}{D_{ax}} \tag{5}$$

For ''closed-open'' and ''closed-closed'' systems, the relations between σ_θ^2 of the system response to a pulse signal and Pe, are given by the Eqs. 6 and 7, respectively.

$$\sigma_\theta^2 = 2\left(\frac{1}{Pe}\right) + 3\left(\frac{1}{Pe}\right)^2 \tag{6}$$

$$\sigma_\theta^2 = 2\left(\frac{1}{Pe}\right) - 2\left(\frac{1}{Pe}\right)^2 (1 - e^{-\mathrm{Pe}}) \tag{7}$$

Simulation Set-Up

Simulation systems

Cold bubbling bed simulations were carried out systematically on two different FCC strippers (empty cylinder and V-baffled). The two strippers are composed of two stage structures, as shown in Figures 1a, b. The size of down cone is Φ600 mm × Φ486 mm × 500 mm and the size of upper cylinder is Φ486 mm × 1500 mm. The empty cylinder stripper has no internals, while the V-baffled stripper has four pairs of V-baffle in the upper cylinder, angled at 45°. Each baffle blocks 50% of the cross-sectional flow area. The simulations in this study were performed at the same conditions as the experiments of Zhang.[41] The gas used was air and the particles were FCC catalysts. The properties of gas and

Table 2. Gas and Particle Properties and Operating Conditions

Particle diameter	58 μm
Particle density	1500 kg/m^3
Air density	1.225 kg/m^3
Air viscosity	1.7×10^{-5} kg/(m s)
Superficial gas velocity	0.10, 0.15, and 0.20 m/s
Catalyst mass flow flux	26.73 kg/(m^2 s)
Catalyst inventory	230 kg

Table 3. Stripping Efficiencies in Different Strippers

Stripper	u_g (m/s)	η (%)
Empty cylinder	0.10	77
V-baffled		92
Empty cylinder	0.15	87
V-baffled		94
Empty cylinder	0.20	86
V-baffled		95

particle and the corresponding experimental conditions are listed in Table 2.

Simulation code and numerical algorithm

Differential equations mentioned in section 2.1 were solved by a finite volume method by Patankar.[42] These equations were discretized by a first-order upwind differencing scheme over the finite volume, and solved by the commercial CFD package Fluent V6.3.26. The drag coefficient of the modified Gidaspow drag model was specified by user-defined functions (UDFs) in the C programming language, and then compiled and hooked to the Fluent solver. The Phase Coupled SIMPLE (PC-SIMPLE) algorithm, which is an extension of the SIMPLE algorithm for multiphase flow, was used for the pressure-velocity coupling and correction.

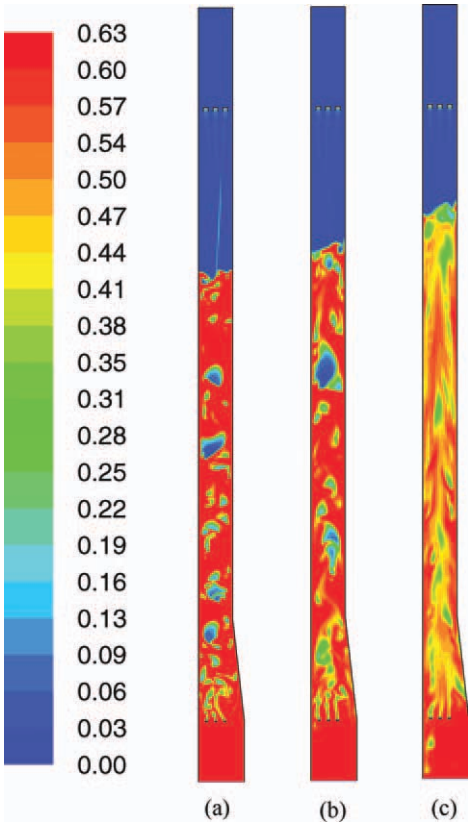

Figure 2. Instantaneous solid volume fractions at three mesh resolutions. (a) 2.5 mm. (b) 5 mm. (c) 7.5 mm.

[Color figure can be viewed in the online issue, which is available at wileyonlinelibrary.com.]

Table 4. Grid Independency Results

Mesh spacing (mm)	2.5	5	7.5	Experiment
α_s ($h = 0.7$ m)	0.552	0.556	0.511	0.56
α_s ($h = 0.9$ m)	0.554	0.555	0.528	0.47
α_s ($h = 1.1$ m)	0.539	0.551	0.531	0.56
α_s ($h = 1.3$ m)	0.552	0.556	0.530	0.51
α_s ($h = 1.5$ m)	0.534	0.54	0.483	0.48
α_s ($h = 1.8$ m)	0.517	0.529	0.503	0.50
Simulation time (h)	168	44	23	

The dimensions of the computational domain were the same as those of the actual experimental fluidized bed. Grids were created in a CAD program called GAMBIT 2.2.30 and exported into Fluent 6.3.26. Additionally, the grid was divided into a lower zone and an upper zone for the purpose of specifying initial conditions.

Because of the usual instability and convergence for multiphase simulation, a very small time step (0.0001 s) with about 20 iterations per time step was used. A convergence criterion of 10^{-3} for each scaled residual component was specified for the relative error between two successive iterations. The total simulation time of gas-solid flow was much longer than the mean solid residence time to ensure to reach the desired operating conditions. The time-averaged distributions of variables were computed covering the period of the last 20 s.

Boundary and initial conditions

The inlet of the gas phase as well as the inlet and outlet of the particulate phase were designated as velocity inlets in Fluent 6.3.26, where the direction of gas or particle flow was normal to the boundary. Flow rates used for each velocity inlet were determined from the superficial velocity mentioned above. The top of the bed was set as the outflow boundary condition for the gas phase. At the wall, no-slip boundary condition is assumed for gas and solid phase.

Initially, the lower zone of stripper was filled with particles at an appropriate initial volume fraction. The initial concentration of the particulate phase was based upon the maximum packing fraction for the material (0.60). The initial velocity of the particulate phase was set at zero.

Results and Discussion

The flow behaviors and stripping efficiencies in the empty cylinder and V-baffled strippers have been successfully investigated in our previous work.[24,25] The results showed that the V-baffled stripper exhibited higher mass transfer rates and overall stripping efficiencies than the empty cylinder stripper, shown in Table 3. However, the details of gas and solids mixing and the effects of gas and solids mixing on stripping efficiency have not been deeply studied. Hereinafter the gas and solid mixing characteristics including bubble size, RTD, backmixing degree, as well as gas/solid flow distribution were further analyzed based on CFD simulation results.

Grid independency

To confirm that the CFD results are independent of the mesh size, a grid independency analysis was carried out using

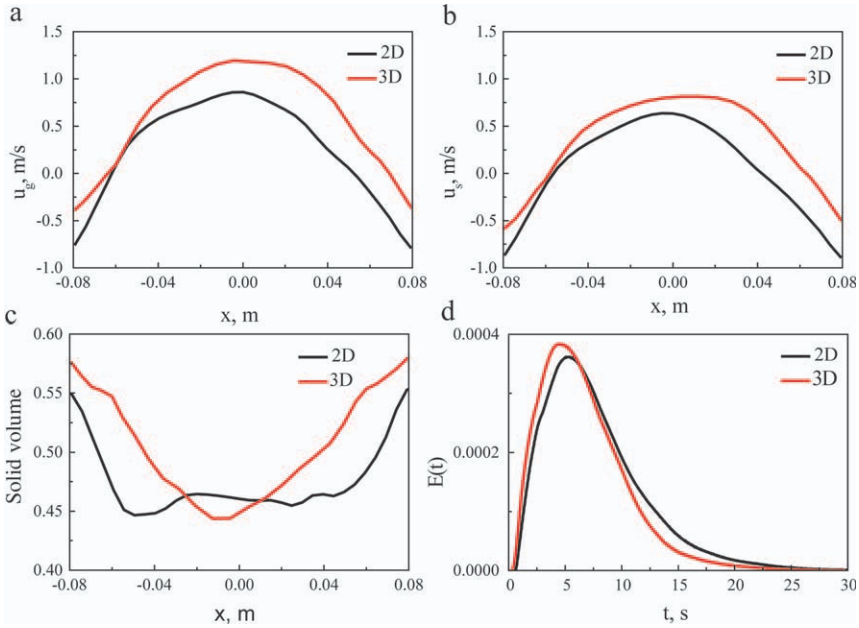

Figure 3. (a) Radial profiles of time-averaged axial gas velocity at 1.0 m. (b) Radial profiles of time-averaged axial solid velocity at 1.0 m. (c) Radial profiles of time-averaged solid volume fraction at 1.0 m. (d) Residence time distributions of gas at the outlet.

[Color figure can be viewed in the online issue, which is available at wileyonlinelibrary.com.]

three mesh interval spacings, i.e., 2.5 mm, 5 mm and 7.5 mm for 20 s of real time simulation. Figure 2 shows the instantaneous solid volume fractions at three mesh resolutions. It can be seen that fine mesh (2.5 mm) case and medium mesh (5.0 mm) case capture more reasonable flow characteristics of bubbles relative to the coarse mesh (7.5 mm). Table 4 shows the prediction of time-averaged solid volume fraction α_s at different axial heights with comparison of the experimental results of Zhang.[41] The α_s obtained from the medium mesh case and fine mesh case are close and are comparable to the experimental data, which indicates that the mesh spacing of 5 mm is sufficiently fine for providing reasonably mesh independent results. Moreover, the simulation time of the mesh with the interval spacing of 5 mm is one fourth of that of 2.5 mm. Therefore, the mesh spacing of 5 mm is used in the current simulation.

Comparison between 2D and 3D results

Two-dimensional (2D) simulation was often used in the open literatures of bubbling fluidized beds simulation. Some research showed 2D simulation could successfully predict the hydrodynamic characteristics in a bubbling bed.[43] However, some papers reported the difference between 2D and 3D simulations.[19] The validity of 2D simulation should be first studied. In this section, the 2D and 3D simulations were carried out and compared. The 2D system dimensions are 0.168 m width and 1.5 m height, and the 3D system dimensions are 0.168 m inner diameter and 1.5 m height. The mesh interval spacing is 5mm. The radial distributions of the time-averaged axial gas, solid velocities and solid volume fraction, as well as the RTD curves of gas obtained from 2D and 3D simulations are compared, as shown in Figure 3. It can be seen that the 2D and 3D simulated results are overall consistent. The calculated mean residence time t_m is 6.2 s in 2D simulation and 7.1 s in 3D simulation, and the dimensionless variance σ_θ^2 is 0.34 in 2D simulation and 0.35 in 3D simulation, respectively. Hence, the mixing extent predicted by the 2D simulation is quantitatively similar with the 3D results. Moreover, the 2D simulation requires lower computational resources. Therefore, the 2D simulation was used in the present work to characterize the gas-solid mixing in FCC strippers.

Bubble size

According to the structural wake model,[44,45] the bubbling fluidized bed is composed of a bubble phase and two particulate phases which are called wake phase and emulsion phase. Bubbles carrying the wakes behind them flow upward in the center region and push the emulsion phase sideways. The emulsion phase is then forced to proceed downward near the wall. Meanwhile, some particles enter the wake phase from the emulsion phase and flow up with bubbles. As the transport resistance is located on the surface of the bubbles, the flow behavior of bubbles is undoubtedly essential to the mass exchange of gas and solids and the final stripping efficiency. Cammarata et al.[46] compared the simulated bubble diameters from 2D and 3D simulations to the calculated diameters from Darton's model.[47] They found that the bubble diameters from both 3D and 2D simulations were close to the diameters from Darton's model which are original from 3D fluidized bed. Thus the 2D diameters in the present simulation can be used to predict the bubble distributions in the actual 3D fluidized bed.

Various definitions have been used to distinguish bubbles in the bubble column such as the local voidage more than 0.7,[48]

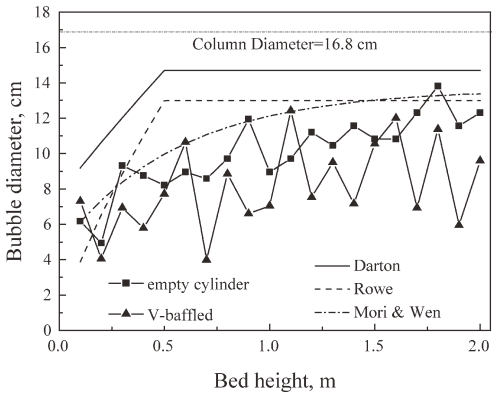

Figure 4. Axial distributions of bubble diameters in different strippers (u_g = 0.15 m/s).

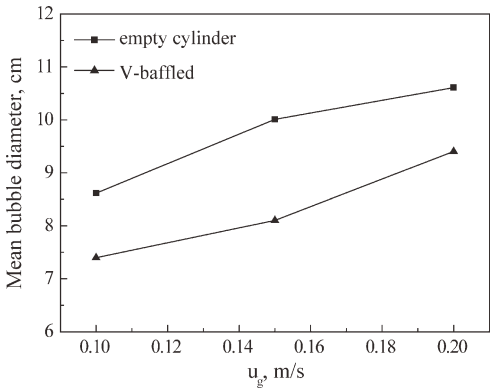

Figure 5. Mean bubble diameters in different strippers.

0.8,[49] and 0.85[50]. Here we adopted the definition of Guenther and Syamlal.[48] The radial distributions of the local voidage α_g at various heights were monitored every 0.01s for 20 s. The radial lengths where α_g is more than 0.7 were regarded as the horizontal bubble sizes. The biggest bubble size at a certain height was recorded as the bubble diameter which was in fact the horizontal length of the biggest bubble passed through this height. The regions below baffles were not regarded as bubbles despite their voidages were close to 1, since they were "dead volumes" useless for mass transfer.[24,25]

The bubble diameters at various heights in the two strippers are presented in Figure 4 and in comparison with D_b calculated by the expressions of Rowe,[51] Darton et al.[47] and Mori and Wen,[52] as shown in Eqs. 8–12, respectively. Relations (8) and (9) take the gas velocity and distributor porosity into account while the relation (10) also considers the effect of fluidized bed diameter. These models, which are based on two-phase theory by Davidson and Harrison, assume that bubbles coalescence along preferred paths, where the distance traveled by two neighboring bubbles before coalescence is proportional to their lateral motion.[46] The bubble diameters calculated from these models, which account for bubble coalescence but not for any splitting, are volumetric average diameters of the biggest bubbles at different heights.

$$D_b = 0.54\ (u_g - u_{mf})^{2/5}(h + h_0)^{4/5} g^{-1/5} \tag{8}$$

$$D_b = (u_g - u_{mf})^{1/2}(h + h_0)^{3/4} g^{-1/4} \tag{9}$$

$$\frac{D_{bm} - D_b}{D_{bm} - D_{b0}} = \exp\ (-0.3\ \ h/D_t) \tag{10}$$

$$D_{b0} = 0.347\ (A_t(u_g - u_{mf})/n_d)^{2/5} \tag{11}$$

$$D_{bm} = 0.652\ (A_t(u_g - u_{mf}))^{2/5} \tag{12}$$

where, D_{bm} is the maximum bubble diameter due to total coalescences of bubbles, and D_{b0} is the initial bubble diameter at the distributor. The parameter h_0 characterizes the distributor. For a porous plate distributor, for example, h_0 is 0.03 m. The minimum fluidizing velocity u_{mf} has a value about 1-3 mm/s,[53] which is negligibly low compared with the superficial gas velocity u_g. For fine Geldart A powders, the growth of bubbles dose not proceed indefinitely and the bubbles reach an equilibrium size at a distance h^* above the distributor. For FCC catalyst particles ($d_p \approx 50\ \mu$m), h^* has a value of about 0.5 m.[54]

Figure 4 indicates the axial distributions of bubble diameters in the two strippers. The diameters calculated from the relations of Rowe[51] and Darton et al.[47] are constants over the height of h^*. The simulated bubble diameters are in reasonable agreement with calculated ones, especially with the data calculated by Mori and Wen's expressions.[52] The agreement demonstrates the feasibility of using CFD method to investigate the bubble performance in the fluidized bed.

At the bottom of the two strippers, the bubbles possess similar diameters of about 5 cm. Approaching to the top of the dense bed, D_b in the empty cylinder stripper increases to about 12 cm, which is about 70% of the column diameter (16.8 cm). This is consistent with the results of Bi and Chen,[55] who reported that the bubble size was restricted to no more than 2/3 bed diameter in the small diameter column. In the V-baffled stripper, the increasing of D_b is restricted because of the redistribution effect of baffles. The sharp fluctuations of D_b indicate the coalescence and breakup of bubbles in the V-baffled stripper. Figure 5 compares the mean bubble diameters in the two strippers. The redistribution effect of the baffles decreases the mean bubble size in the V-baffled stripper to about 80% of that in the empty cylinder stripper, which is helpful for increasing the interfacial area and thus improving the stripping efficiency. O'Dowd et al.[21] has reported that the interfacial area was larger in the baffled column at low velocities compared to the open column.

Table 5 lists the mean bubble diameters in the empty cylinder and V-baffled stripper. It can be seen from Tables 3 and 5 that the V-baffled stripper with smaller bubble diameters exhibits higher stripping efficiencies. Thus an effective

Table 5. Mean Bubble Diameters in Different Strippers

Stripper	u_g (m/s)	D_b (cm)
Empty cylinder	0.10	8.6
V-baffled		7.4
Empty cylinder	0.15	10.0
V-baffled		8.1
Empty cylinder	0.20	10.6
V-baffled		9.4

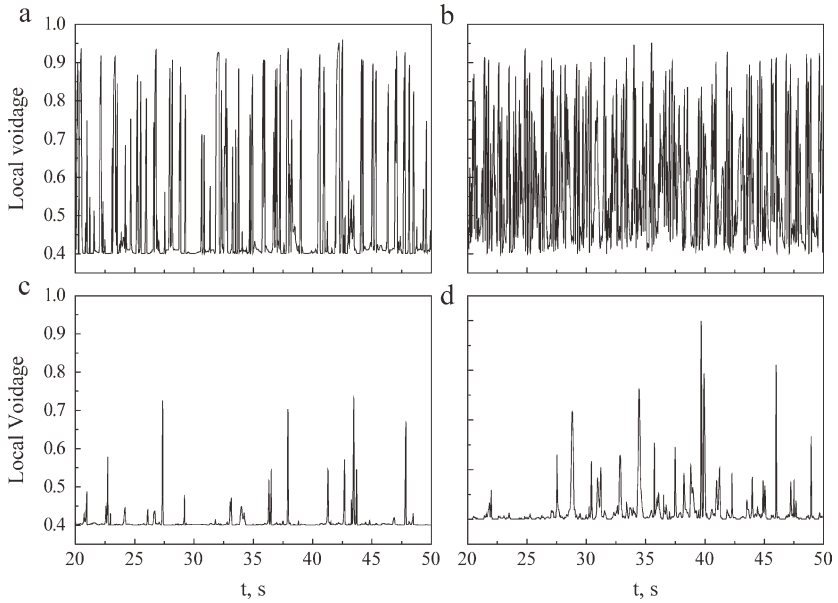

Figure 6. Local voidage fluctuations (u_g = 0.15 m/s, h = 1.0 m).

(a) empty cylinder stripper, $x = 0$ mm. (b) V-baffled stripper, $x = 0$ mm. (c) empty cylinder stripper, $x = 76$ mm. (d) V-baffled stripper, $x = 76$ mm.

method to increase stripping efficiency is reducing the bubble diameter to increase the interfacial area of mass transfer. Until now, many kinds of internals such as grid[56] and packed[57] structures have been introduced in FCC strippers to restrict the growth of bubbles and improve gas-solid contacting. However, the subdivision of stripping column brings more difficulties on the maintenance of apparatus. The optimization of simple structures is more practical, but need deeper understanding of the influence of the gas-solid mixing on the stripping efficiency.

Characteristics of transient local voidage and axial velocities

The distributions of gas and solids in the bubble and emulsion phase have an essential effect on mass transfer. Figure 6 shows the voidage-time curves in the center ($x = 0$ mm) and near the wall ($x = 76$ mm) of the two strippers. The local voidages show random and fluctuating from ε_{mf} to 1 at a given position, and the fluctuations of the local voidage in the center are more violent than that near the wall. To quantitatively analyze the local fluctuation characteristics, the probability density function of the voidage varying from ε_{mf} to 1 was introduced. The probability for the voidage to fall within a particular region is given by the integral of the voidage's density over the region. Figure 7 depicts the probability density functions of local voidage at two radial locations. In Figure 7 (a), the peak near the voidage of 0.4 in the empty stripper represents the emulsion phase. The peak value is about 37%. In the V-baffled stripper, the peak position for the emulsion phase moves to a higher voidage, indicating more gas entering the emulsion phase. Besides, the peak value for the emulsion phase is much lower, about 7%. The compensation is the intensification of the wake phase from the voidage 0.5 to 0.7. This is helpful for promoting the mass transfer between the bubble and emulsion phase. In the wall regions of both strippers, as shown in Figure 7b, the peak value is as high as 50 and 80%, respectively, because of the domination of the emulsion phase.

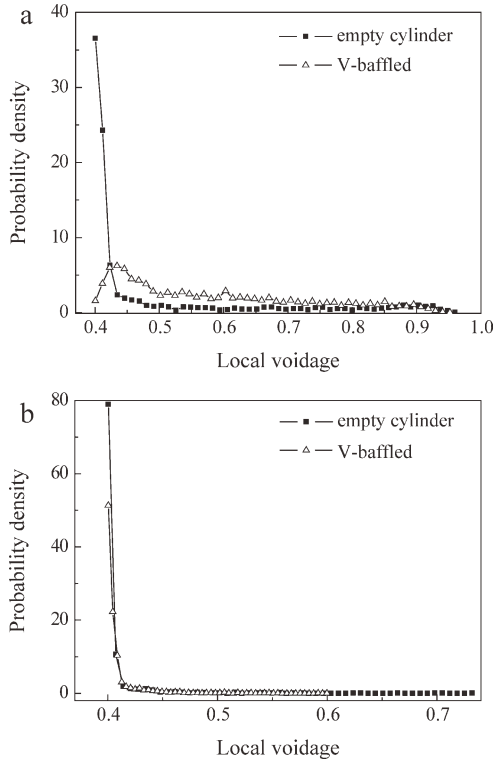

Figure 7. Probability density distributions of local voidage (u_g = 0.15 m/s, h = 1.0 m).

(a) $x = 0$ mm. (b) $x = 76$ mm.

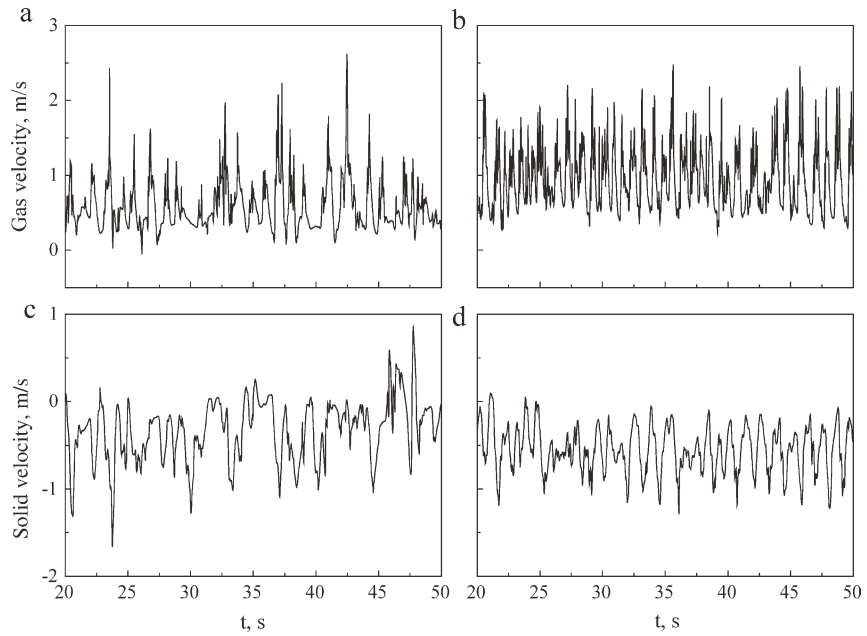

Figure 8. Axial velocity fluctuations (u_g = 0.15 m/s, h = 1.0 m).

(a) empty cylinder stripper, gas, $x = 0$ mm. (b) V-baffled stripper, gas, $x = 0$ mm. (c) empty cylinder stripper, solid, $x = 76$ mm. (d) V-baffled stripper, solid, $x = 76$ mm.

Figure 8 shows the axial velocity fluctuations of gas and solids in the center and near wall region. The velocities of gas are mainly positive in the center and those of solids are mainly negative near the wall because of the core-annular flow structure. In the center region, the calculated time-averaged gas velocity is 0.55 m/s in the empty cylinder stripper and 0.28 m/s in the V-baffled stripper. In the near wall region, the calculated time-averaged solid velocity is −0.24 m/s in the empty cylinder stripper and −0.36 m/s in the V-baffled stripper.

The probability density functions of axial velocities of gas in the center and solids near the wall are plotted in Figure 9. Like the probability density of voidage, the probability density distribution of gas/solid velocity can be used to quantitatively represent the probability for the velocity to fall within a specific region. It can be seen that bubbles flow upward in the center region, leading to about 100% gas processing upward at $x = 0$ mm in both strippers. The probability of the gas velocity in the center of the V-baffled stripper exhibits a double-peak distribution compared to the single-peak distribution in the empty cylinder stripper. This double-peak in the V-baffled stripper indicates the existence of more fractions of wakes and more small bubbles. According to Figure 9b, the probability for the velocity higher than 0 m/s, i.e., the probability of solids back-mixing near the wall, in the V-baffled stripper is only 1% but that in the empty cylinder stripper is as high as 13%. The reduction of axial back-mixing in the V-baffled stripper will definitely increase the driving force of mass transfer and improve the stripping efficiency.

RTDs of gas and solid

The RTD curve is an indication of flow behavior to determine the mixing degree. For the ideal plug flow, all fluid elements have equal residence times at the outlet and the RTD curve is a vertical line after the injection time. For the ideal mixing flow, the fluid is completely mixed and the RTD curve at the outlet increases abruptly in an instantaneous rise at the injection time and decay exponentially with time thereafter.[58]

Figures 10 and 11 show the RTD curves of gas and solids in both strippers. The delay of the increase from time zero and the single-peak distribution indicates the combination of the plug and mixing flow. It can be seen that all curves of gas and solids exhibit long tails. Harris et al.[59] suggested that sharp peak and long tail were indicative of a core-annulus flow structure. The long tails are caused by the recirculation of gas and solids. The RTD curves of the gas in the two strippers and those of the solids in the V-baffled stripper become narrower and higher with increasing gas velocity. However, for the solids in the empty cylinder stripper, the RTD curves show similar distributions at different velocities. We attribute this trend to the significant back-mixing of solids in the empty cylinder stripper. The increasing degree of the solid back-mixing with increasing gas velocity is so great that it offsets the increasing degree of the solid velocity.

To investigate further into the mixing phenomena in the two strippers, the global and local mixing degrees were quantified in the next two sections.

Global mixing of gas and solid

The characteristic parameters of RTD curves such as dimensionless variance σ_0^2 and Peclet number Pe are capable of quantifying the global mixing degree in the fluidized bed. And the mean residence time t_m can reflect the fraction of flow trapped in the recirculation pattern.

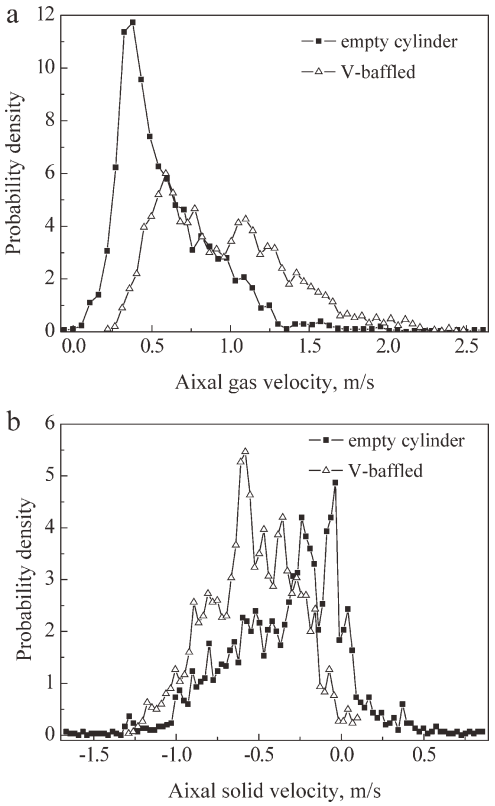

Figure 9. Probability density distributions of axial velocity (u_g = 0.15 m/s, h = 1.0 m).

(a) gas, x = 0 mm. (b) solid, x = 76 mm.

In Figures 12 and 13, t_m and σ_θ^2 in the two strippers are plotted as functions of superficial gas velocity. The σ_θ^2 of gas and solids in the two strippers are all more than 0.2, which indicate the flow deviating from the plug flow. The σ_θ^2 of gas in the V-baffled stripper is between 0.2 and 0.3 which is less than that in the empty cylinder stripper. The σ_θ^2 of solids in the empty cylinder stripper is as high as 0.7 at 0.2 m/s which is 2.5 times the σ_θ^2 in the V-baffled stripper. It is proved that the existence of V-baffles effectively inhibits the solid back-mixing. Due to the severe back-mixing of solids, the catalysts in the empty cylinder stripper undergo multiple recirculations and the t_m of solids is thus prolonged, as shown in Figure 13. The t_m of solids in the empty cylinder stripper at 0.20 m/s is two times of that in the V-baffled stripper. The reverse change of the t_m of solids in the empty cylinder stripper compared to that in the V-baffled stripper can also explain the particular change of RTD of solid in Figure 11a.

The long residence time and low back-mixing degree of catalysts in FCC strippers are favorable for increasing stripping efficiency. The empty cylinder stripper had long residence time, but meanwhile had more back-mixing. The low stripping efficiency of empty cylinder stripper showed that the back-mixing of catalysts had more influence on the stripping efficiency than the residence time. Thus, it is more important to compare the back-mixing degree than to compare the mean residence time when comparing the stripping efficiency from the RTD curves.

The RTD curves of gas and solids are also related to the gas-solid mixing in the frame of the classic chemical engineering approach with axial dispersed model as introduced previously. The obtained Peclet number can describe directly the local back-mixing degree, as shown in Figure 14. The countercurrent flow of the stripping gas and catalysts leads to severe back-mixing in the strippers. Almost all Peclet numbers in the two strippers are less than 11, which were very comparable to the results of Lorences et al.[13] who found that the Pe of gas in the gas-solid bubbling bed was close to 10, and the Pe in the column with internals was higher than in the open column. The Pe of gas in the V-baffled stripper is about 10, which is 1.12 times of that in the empty cylinder stripper. The Pe of solids in the V-baffled stripper is close to 6, which is 26 times of that in the empty cylinder stripper. Higher Peclet numbers in the V-baffled stripper corresponds to higher stripping efficiencies as shown in Tables 3 and 6. The redistribution effect of the baffled structure on the back-mixing of gas and solids leads to higher Pe in the V-baffled stripper. Such effect of baffles on the axial dispersion was also proved by Zhang et al.[23]

Local mixing of solid

To investigate the detail of the local back-mixing, the local back-mixing index (LBI) is introduced. It is defined as the ratio of the back-mixed mass flow to the total mass flow at a certain position,[60] shown as the following,

$$\mathrm{LBI} = \frac{\sum_{t=t_1}^{t_2} \rho u_y^+}{\sum_{t=t_1}^{t_2} \left(\rho u_y^+ + \left| \rho u_y^- \right| \right)} \tag{13}$$

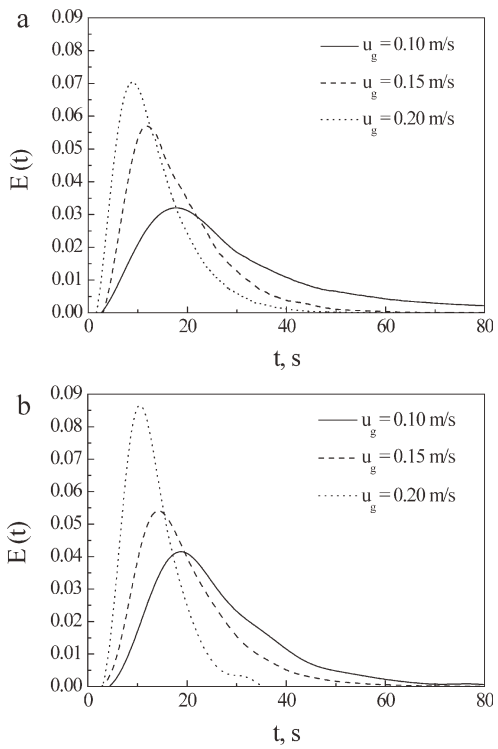

Figure 10. Residence time distributions of gas.

(a) empty cylinder stripper. (b) V-baffled stripper.

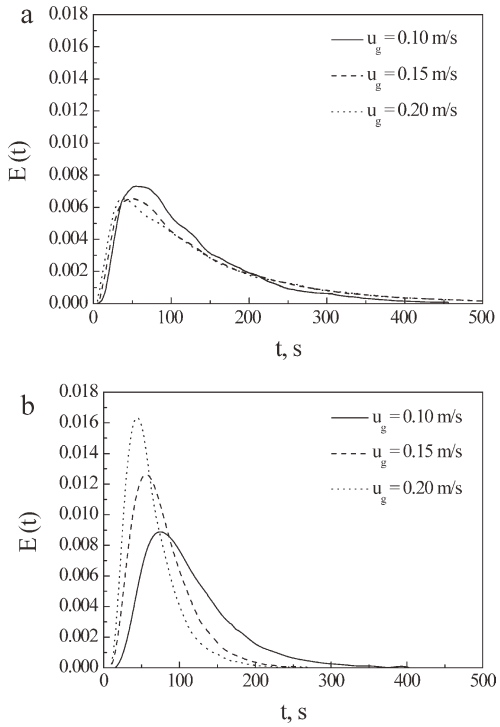

Figure 11. Residence time distributions of solid.

(a) empty cylinder stripper. (b) V-baffled stripper.

The u_y^+ and u_y^- of solids were recorded every 0.01 s for 20 s. LBI ranges from 0 (no back-mixing) to 1 (complete back-mixing). The obtained LBI at different positions in the empty cylinder and V-baffled stripper are shown in Figure 15. As the bubbles move mainly in the center region, carrying catalysts in the bubble wakes, the LBI of solids in the center is close to 1. The wall region is the main downwardly flowing route of the catalysts, thus the LBI of solids is close to 0. In the empty cylinder stripper, the LBI of solids at different heights show similar symmetric distributions. But in the V-baffled stripper, the LBI of solids show asymmetrical distributions except on the height of 1.3 m which has an equal distance from the upper and lower baffles.

In the V-baffled stripper, the positions of 0.5, 1.0, 1.4, 1.5 and 2.0 m are near to the left baffles ($x < 0$ mm) while relatively far from the right baffles ($x > 0$ mm). It can be seen that the LBI at $x = -42$ mm are lower than 0.4 and the LBI at $x = 42$ mm are higher than 0.6. All the LBI at these positions in the empty cylinder stripper are close to 0.6. The back-mixing of the solids seems stronger at $x = 42$ mm in the V-baffled stripper than in the empty cylinder stripper. But the solid back-mixing will be damped to lower than 0.4 as the catalysts proceed to the upper baffles. Overall, the asymmetrical distributions of LBI arising from staggered arrangement of baffles effectively reduce the global back-mixing of catalysts.

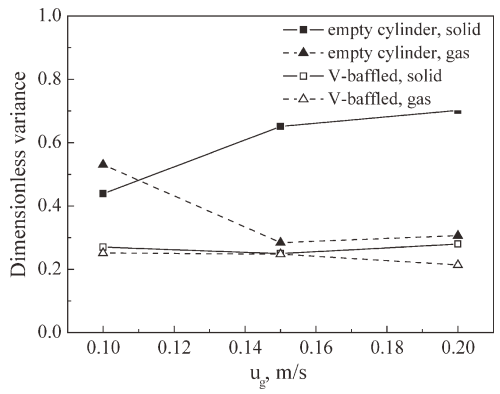

Figure 12. Dimensionless Variances of gas and solid.

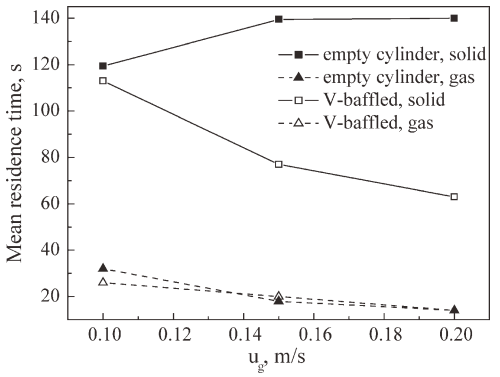

Figure 13. Mean residence times of gas and solid.

Traditionally, the improvement of the stripper structures is based on the following principles: decreasing the residence time and back-mixing degree of gas, increasing the residence time of solids while decreasing the solid back-mixing degree. The application of multistage stripping structure[61,62]

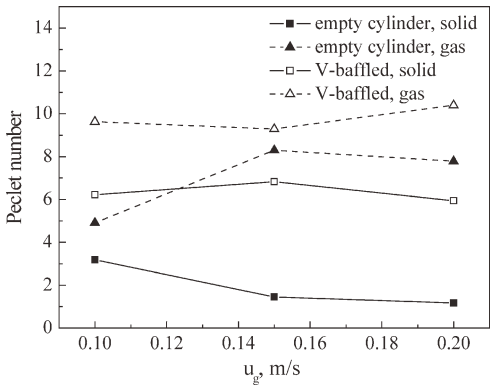

Figure 14. Peclet numbers of gas and solid.

Table 6. Peclet Numbers in Different Strippers

Stripper	u_g (m/s)	Pe_p	Pe_g
Empty cylinder	0.10	3.2	4.9
V-baffled		6.2	9.6
Empty cylinder	0.15	1.4	8.3
V-baffled		6.8	9.3
Empty cylinder	0.20	1.2	7.8
V-baffled		5.9	10.4

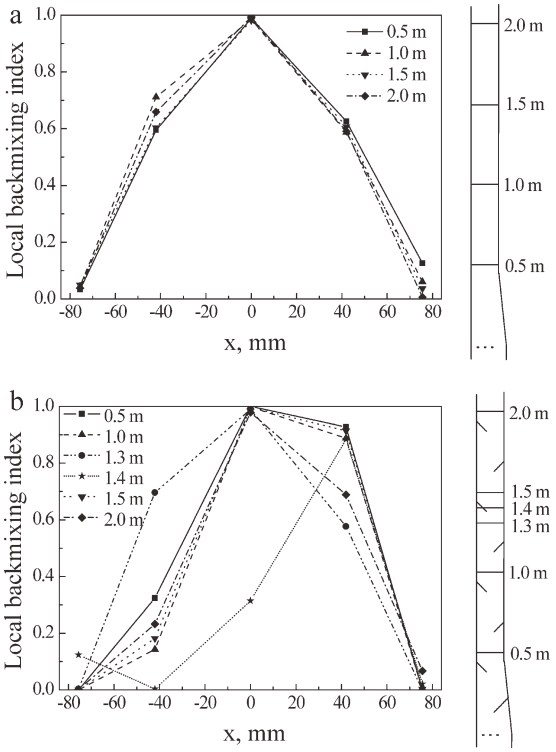

Figure 15. Local back-mixing index at various axial positions.

(a) empty cylinder stripper. (b) V-baffled stripper.

can prolong the residence time without increasing the back-mixing. But the stripper volume is enlarged and the stripper structure is becoming complicated. Another promising stripper which has a simple structure and does not enlarge the stripper volume is the so-called "annular stripper,"[63] which was proved to have a high stripping efficiency by experiments. The details of gas and solids mixing and their effect on stripping efficiency in the annular stripper deserve in-depth investigation by the above approach.

Conclusions

CFD simulation was performed for two kinds of FCC strippers to study the gas and solids mixing using Eulerian–Eulerian two-fluid model, RTD model and axial dispersion model. The simulation results revealed that comparing to the empty cylinder stripper, the V-baffled stripper has the following advantages to improve the stripping efficiency:

(1) The bubble coalescence and break-up is strengthened. And the mean bubble diameter is decreased to about 80% of that in the empty cylinder stripper.

(2) The wake phase is intensified which will strengthen the mass transfer between the bubble and emulsion phase.

(3) The global back-mixing degree is reduced. The probability of solids back-mixing near the wall of 1% in the V-baffled stripper is much lower than that of 13% in the empty cylinder stripper. The *Pe* of gas in the V-baffled stripper is 1.1–2 times of that in the empty cylinder stripper. And the *Pe* of solids is 2–6 times of that in the empty cylinder stripper.

(4) The local back-mixing extent in the V-baffled stripper exhibits asymmetrical distribution because of the staggered arrangement of baffles, which effectively reduce the global back-mixing of catalysts.

The obtained results highlight the principles of stripper optimization on increasing stripping efficiency.

Acknowledgments

The authors acknowledge the support by the National Natural Science Foundation of China through the program for Distinguished Young Scholar (Grant No. 20725620) and the National Basic Research Program (Grant No. 2010CB226906).

Notation

A_t = cross-sectional area of the fluidized bed, m^2
C_D = drag coefficient
d_p = diameter of particle, m
$d_p^* d_p^*$ = effective mean diameter of particle, m
D = diffusion coefficient, $m^2\ s^{-1}$
D_{ax} = axial dispersion coefficient, $m^2\ s^{-1}$
D_b = diameter of bubble diameter, m
D_{b0} = initial bubble diameter at the distributor, m
D_{bm} = maximum bubble diameter, m
D_t = fluidized bed diameter, m
e = restitution coefficient
$E(t)$ = residence time distribution, s^{-1}
g = gravity acceleration, $m\ s^{-2}$
g_0 = radial distribution function
h = bed height, m
h_0 = bed height characterizing the distributor, m
h^* = bed height where bubble reaching equivalent diameter, m
L = distance between the tracer input and detection points, m
LBI = local backmixing index
n_d = number of orifice opening in the distributor
p = pressure, Pa
Pe = Peclet number
r = radial position, m
R = bed radius, m
Re = Reynolds number
t = time, s
t_m = mean residence time, s
u = velocity, $m\ s^{-1}$
$\vec{u}$ = velocity vector, m/s
u_g = superficial gas velocity, m/s
u_{mf} = minimum fluidization velocity, m/s
$u_y^+ u_y^+$ = axial velocity of up-flowing fluid, m/s
$u_y^- u_y^-$ = axial velocity of down-flowing fluid, m/s
x = direction coordinate
Y_n = mass fraction of species n, wt %

Greek letters

A = void fraction
β = interphase momentum exchange coefficient, $kg/(m^3\ s)$
γ_Θ = collisional dissipation of energy, $kg/(m\ s^3)$
θ = dimensionless time
λ_p = solid bulk viscosity, Pa s
μ_p = particle phase shear viscosity, Pa s
ρ = density, kg/m^3
σ_t^2 = variance of the standard deviation, s^2
σ_θ^2 = dimensionless variance
τ = stress tensor, Pa
Γ_Θ = diffusion coefficient for the energy fluctuation, kg/(m s)
Θ = granular temperature, m^2/s^2

Subscripts

i, j, k = direction coordinate
g = gas phase
m = mean

max = maximum
n = species n
p = particle phase

Literature Cited

1. Nguyen HV, Whitehead AB, Potter OE. Gas mixing, solids movement, and bubble activities in large scale fluidized beds. *AIChE J*. 1977;23:913–922.
2. Krishna R, Van Baten JM. Using CFD for scaling up gas-solid bubbling fluidized bed reactors with Geldart A powders. *Chem Eng J*. 2001;82:247–257.
3. Basesme EA, Levy EK. Solids exchange between the bubble wake and the emulsion pahse in a two-dimensional gas-fluidized bed. *Powder Technol*. 1992;72:45–50.
4. Wu W, Agarwal PK. The effect of bed temperature on mass transfer between the bubble and emulsion phases in a fluidized bed. *Can J Chem Eng*. 2003;81:940–948.
5. Krishna R, Van Baten JM. Mass transfer in bubble columns. *Catal Today*. 2003;79–80:67–75.
6. Behkish A, Men Z, Inga RJ, Morsi BI. Mass transfer characteristics in a large-scale slurry bubble column reactor with organic liquid mixtures. *Chem Eng Sci*. 2002;57:3307–3324.
7. Kantarci N, Borak F, Ulgen KO. Bubble column reactors. *Process Biochem*. 2005;40:2263–2283.
8. Wolf D, Resnick W. Experimental study of residence time distribution in multistage fluidized bed. *Ind Eng Chem Fund*. 1965;4:77–81.
9. Sotudeh-Gharebaagh R, Chaouki J. Gas mixing in a turbulent fluidized bed reactor. *Can J Chem Eng*. 2000;78:65–74.
10. Du B, Fan L-S, Wei F, Warsito W. Gas and solids mixing in a turbulent fluidized bed. *AIChE J*. 2002;48:1896–1909.
11. Zhong W, Xiao R, Zhang M. Experimental study of gas mixing in a spout-fluid bed. *AIChE J*. 2006;52:924–930.
12. Smolders K, Baeyens J. Overall solids movement and solids residence time distribution in a CFB-riser. *Chem Eng Sci*. 2000;55:4101–4116.
13. Lorences M J, Laviolette J-P, Patience GS, Alonso M, Díez FV. Fluid bed gas RTD: effect of fines and internals. *Powder Technol*. 2006;168:1–9.
14. Cui HP, Strabel M, Rusnell D, Bi HT, Mansaray K, Grace JR, Lim CJ, McKnight CA, Bulbuc D. Gas and solids mixing in a dynamically scaled fluid coker stripper. *Chem Eng Sci*. 2006;61:388–396.
15. Xia YK, Peng FF, Wolfe E. CFD simulation of alleviation of fluid back mixing by baffles in bubble column. *Chem Eng Sci*. 2006;19:925–937.
16. Moullec YL, Potier O, Gentric C, Leclerc JP. Flow field and residence time distribution simulation of a cross-flow gas-liquid wastewater treatment reactor using CFD. *Chem Eng Sci*. 2008;63:2436–2449.
17. Bakhtier TA, Farouk B, Haas CN. Countercurrent gas/liquid flow and mixing: implications for water disinfection. *Int J Multiphase Flow*. 2009;35:171–184.
18. Andreux R, Petit G, Hemati M, Simonin O. Hydrodynamic and solid residence time distribution in a circulating fluidized bed: experimental and 3D computational study. *Chem Eng Process*. 2008;47:463–473.
19. Li T, Zhang Y, Grace JR, Bi X. Numerical investigation of gas mixing in gas-solid fluidized beds. *AIChE J*. 2010;56:2280–2296.
20. Wang Q, Zhang K, Sun G, Brandani S, Gao J, Jiang J. CFD simulation of fluid dynamic in a gas-solid jetting fluidized bed. *Int J Chem React Eng*. 2007;5:A112.
21. O'Dowd W, Smith DN, Ruether JA, Saxena SC. Gas and solids behaviors in a baffled and unbaffled slurry bubble column. *AIChE J*. 1987;33:1959–1970.
22. Cui H, Grace J, McKnight C, Zhang T. Jet configuration for improved fluidized bed stripping. *Chem Eng J*. 2006;125:1–8.
23. Zhang Y, Lu C, Shi M. Evaluating solids dispersion in fluidized beds of fine particles by gas backmixing experiments. *Chem Eng Res Des*. 2009;87:1400–1408.
24. Gao JS, Chang J, Lan XY, Yang Y, Xu CM, Lu CX. CFD modeling of mass transfer and stripping efficiency in FCCU strippers. *AIChE J*. 2008;54:1164–1177.
25. Gao JS, Chang J, Xu CM, Lan XY, Yang Y. CFD simulation of gas solid flow in FCC strippers. *Chem Eng Sci*. 2008;63:1827–1841.
26. Jenkins JT, Savage SB. A theory for the rapid flow of identical, smooth, nearly elastic, spherical particles. *J Fluid Mech*. 1983;30:187–202.
27. Sinclair JL, Jackson R. Gas-particle flow in a vertical pipe with particle-particle interactions. *AIChE J*. 1989;35:1473–1496.
28. Gidaspow D. *Multiphase Flow and Fluidization: Continuum and Kinetic Theory Descriptions*. San Diego: Academic Press, 1994.
29. Syamlal M, O'Brien TJ. Computer simulation of bubbles in fluidized beds. *AIChE Symp Ser*. 1989;85:22–31.
30. Lu H, He Y, Gidaspow D. Hydrodynamic modelling of binary mixture in a gas bubbling fluidized bed using the kinetic theory of granular flow. *Chem Eng Sci*. 2003;58:1197–1205.
31. Ergun S. Fluid flow through packed columns. *Chem Eng Prog*. 1952;48:89–94.
32. Wen CY, Yu YH. Mechanics of fluidization. *Chem Eng Prog Sym Ser*. 1966;62:100–111.
33. Lettieri P, Brandani S, Yates JG, Newton D, A generalization of the Foscolo and Gibilaro particle-bed model to predict the fluid bed stability of some fresh FCC catalysts at elevated temperatures. *Chem Eng Sci*. 2001;56:5401–5412.
34. Danckwerts PV. Continuous flow systems: distribution of residence times. *Chem Eng Sci*. 1953;2:1–13.
35. Levenspiel O, Smith WK. Notes on the diffusion-type model for the longitudinal mixing of fluids in flow. *Chem Eng Sci*. 1957;6:227–235.
36. Xu M, Finch JA. The axial dispersion model in flotation column studies. *Miner Eng*. 1991;4:553–562.
37. Sivashanmugam P, Sundaram S. Residence time distribution studies in annular circulating fluidised bed drier. *Powder Technol*. 2000;107:256–258.
38. Bardin-Monnier N, Guiraud P, Gourdon C. Residence time distribution of droplets within discs and doughnuts pulsed extraction columns via Lagrangian experiments and simulations. *Chem Eng J*. 2003;94:241–254.
39. Zahradník J, Fialová M. The effect of bubbling regime on gas and liquid phase mixing in bubble column reactors. *Chem Eng Sci*. 1996;51:2491–2500.
40. Grasa G, Abanades JC. The use of two different models to describe the axial mixing of solids in fluidised beds. *Chem Eng Sci*. 2002;57:2791–2798.
41. Zhang YM. Study on the Gas-Solid Flow in FCCU Stripper. M.Sc. Thesis. Beijing: China University of Petroleum, 2003.
42. Patankar SV. *Numerical Heat Transfer and Fluid Flow*. New York: Hemisphere Publishing Corporation, 1980.
43. Xie N, Battaglia F, Pannala S. Effects of using two- versus three-dimensional computational modeling of fluidized beds Part I, hydrodynamics. *Powder Technol*. 2008;182:1–13.
44. Tang WT, Fan LS. Hydrodynamics of a three-phase fluidized bed containing low-density particles. *AIChE J*. 1989;5:355.
45. Murry P, Fan LS. Axial solid distribution in slurry bubble columns. *Ind Eng Chem Res*. 1989;28:1697.
46. Cammarata L, Lettieri P, Micale GDM, Colman D. 2D and 3D CFD simulations of bubbling fluidized beds using Eulerian-Eulerian models. *Int J Chem React Eng*. 2003;1:A48.
47. Darton R, LaNauze RD, Davidson JF, Harrison D. Bubble growth due to coalescence in fluidized beds. *Trans Inst Chem Eng*. 1977;55:274–280.
48. Guenther C, Syamlal M. The effect of numerical diffusion on simulation of isolated bubbles in a gas–solid fluidized bed. *Powder Technol*. 2001;116:142–154.
49. Xu X, Xiang WG, Qin CH. Numerical simulation of flow characteristics in the dense-phase zone of a fluidized bed. *J Eng Therm Energy Power*. 2004;19:131–133.
50. Nienwland JJ, Veenendaal ML, Kuipers JAM. Bubble formation at a single orifice in gas fluidized beds. *Chem Eng Sci*. 1996;51:4087–4126.
51. Rowe PN. Prediction of bubble size in a gas fluidised bed. *Chem Eng Sci*. 1976;31:285–288.
52. Mori S, Wen CY. Estimation of bubble diameter in gaseous fluidized beds. *AIChE J*. 1975;21:109–115.
53. Lu CX, Wang ZA. *Fluidization Technology of Fluid Catalytic Cracking*. Beijing: China Petrochemical Press, 2002.
54. Ellenberger J, Krishna R. A unified approach to the scale up of gas-solid fluidized and gas-liquid bubble column reactors. *Chem Eng Sci*. 1994;49:5391–5411.

55. Bi H, Chen A. Presure fluctuations in gas-solids fluidized beds. *Chin Particuol*. 2003;1:139–144.
56. Rall RR. Apparatus for contacting of gases and solids in fluidized beds. USP 6224833, 2001.
57. Senegas M-A, Patureaus T, Selem P, Mauleon J-L. Process and apparatus for stripping fluidized and use thereof in a fluid cracking process. USP 5716585, 1998.
58. Choi BS, Wan B, Philyaw S, Dhanasekharan K, Ring TA. Residence time distributions in a stirred tank: comparison of CFD predictions with experiment. *Ind Eng Chem Res*. 2004;43:6548–6556.
59. Harris AT, Davidson JF, Thorpe RB. Particle residence time distributions in circulating fluidised beds. *Chem Eng Sci*. 2003;58:2181–2202.
60. Yan CY. Gas-solid flow behavior in a compound fluidized bed petroleum coke combustor. Ph.D. thesis. Beijing: China University of Petroleum, 2007.
61. Zhang Z, Tian G. Development of multi-stage combination stripper for FCC spent catalyst. *Petro Refinery Eng*. 2006;36:12–16.
62. Van Kleeck David A, Hardesty Donald E. Stage catalyst concentric annular stripper. USP 5260034, 1993.
63. Lu CX, Liu MX, Shi MX. Efficient regenerated catalyst stripping apparatus. ZL 00259076.X, 2001.

Manuscript received July 25, 2010, revision received Feb. 6, 2011, and final revision received Mar. 31, 2011.